Simulation of electrophoretic stretching of DNA in a microcontraction using an obstacle array for conformational preconditioning

Citation: Trahan, Daniel W., and Patrick S. Doyle. "Simulation of electrophoretic stretching of DNA in a microcontraction using an obstacle array for conformational preconditioning." Biomicrofluidics 3.1 (2009): 012803-14. © 2009 American Institute of Physics.

As Published: http://dx.doi.org/10.1063/1.3055275

Publisher: American Institute of Physics

Persistent URL: http://hdl.handle.net/1721.1/60669

Version: Final published version: final published article, as it appeared in a journal, conference proceedings, or other formally published context

Simulation of electrophoretic stretching of DNA in a microcontraction using an obstacle array for conformational preconditioning

Daniel W. Trahan and Patrick S. Doyle[a)]
Department of Chemical Engineering, Massachusetts Institute of Technology, Cambridge, Massachusetts 02139, USA

(Received 30 September 2008; accepted 20 November 2008; published online 7 January 2009)

Recently our group has reported experiments using an obstacle array to precondition the conformations of DNA molecules to facilitate their stretch in a microcontraction. Based upon previous successes simulating electrophoretic stretching in microcontractions without obstacles, we use our simulation model to study the deformation of DNA chains in a microcontraction preceded by an array of cylindrical obstacles. We compare our data to the experimental results and find good qualitative, and even quantitative, agreement concerning the behavior of the chains in the array; however, the simulations overpredict the mean stretch of the chains as they leave the contraction. We examine the amount of stretch gained between leaving the array and reaching the end of the contraction and speculate that the differences seen are caused by nonlinear electrokinetic effects that become important in the contraction due to a combination of field gradients and high field strengths. © *2009 American Institute of Physics.* [DOI: 10.1063/1.3055275]

I. INTRODUCTION

Biological studies have long relied on the genetic information encoded within DNA molecules. Traditionally, this information is extracted using sequencing techniques, such as gel electrophoresis, that provide single base-pair resolution.[1] While often extraordinarily powerful for molecular biological studies, genetic information at this level of detail is unnecessary for many applications. An often used alternative is DNA mapping which provides lower-resolution genomic information. But the state-of-the-art mapping scheme still requires multiple sets of restriction enzymes and numerous separations by gel electrophoresis.[2] Such techniques are time consuming and expensive, and these drawbacks have spurred interest in mapping technologies that are not based on gel separations.

One such method is direct linear analysis[2,3] (DLA) which involves measuring the physical distance between specific sequences along the DNA backbone. This measurement gives a simple and direct physical map of the molecule without the use of restriction enzymes or separation techniques.[2–4] In DLA, the strands are tagged with sequence-specific fluorescent probes, stretched to their full contour length, and passed by an optical sensor that measures the distance between the probes. The main obstacle in implementing DLA is that the DNA strands, which at equilibrium are entropically coiled,[5] must be fully stretched in order for the measured distance between probes to have a physically relevant meaning.

Many ways have been developed to stretch DNA. Some involve changing the equilibrium conformation from a coil to a more elongated structure by confining DNA.[6,7] Others have attached beads to the ends of DNA and applied forces directly to the molecule using magnetic[8,9] or optical

[a)]Electronic address: pdoyle@mit.edu.

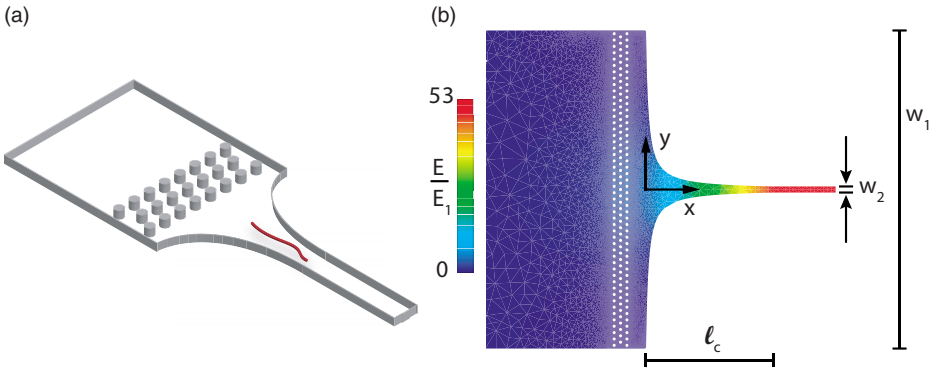

FIG. 1. (a) A cartoon schematic of the general composition of the stretching device (not drawn to scale). The red line represents a strand of DNA stretching as it moves through the contraction. (b) The FEM solution for the magnitude of the electric field normalized by the value of the electric field at the channel inlet (E_1).

traps.[10,11] Collisions with microfabricated obstacles have also been shown to linearize DNA.[12–14] But a very practical method for simple, inexpensive, high-throughput devices is using field gradients to deform the molecules.[15,16]

In DLA devices, the molecules are typically stretched by field gradients in microcontractions.[2,3,17–20] However, in these strain-limited devices, molecular individualism[21] leads to a large population of molecules that do not reach full extension. Recent studies have shown that the effects of molecular individualism can be mitigated by "preconfiguring" the initial conformation of a molecule before it is stretched.[18,20,22] Several different methods to preconfigure molecules have been shown to increase the uniformity of stretch, including preshearing[22] and passing through a gel matrix.[18] A promising technique is placing a microfabricated obstacle array just before the contraction to induce molecular collisions with the obstacles[4,20] [see Fig. 1(a)]. The collision of DNA with a post often leads to hooking events that change the conformation of the molecules thereby reducing the proportion of slowly stretching conformations. The collision of a DNA molecule with a single post is a well-studied problem both experimentally[23–25] and numerically.[26–28] Several qualitatively different types of hooks have been identified,[25] and their stretching and unhooking dynamics have been investigated.[25,28] The effect of large arrays of posts has been considered as well, with studies focussed on the start-up behavior of the molecules as they enter the array[14] and their subsequent steady-state behavior.[29–31] Placing a post array just before the contraction to preconfigure the molecules is also advantageous because the resulting device is simple to fabricate, reusable, and easily scaled.

Previously, Kim and Doyle[32] developed a simulation method to study DNA electrophoresis in complex device geometries with nonhomogeneous electric fields. They have shown that this model can accurately predict experimental results, even at a quantitative level, for the cases of DNA stretching in microcontractions without posts[19] and the collision of a DNA molecule with a single post in a uniform field.[28] The previous success of the model leads us to consider whether or not it will be useful in studying the effects of placing an obstacle array in front of a microcontraction.

The objectives of this study are to use the numerical model of Kim and Doyle[32] to predict the stretching behavior of DNA molecules in a microdevice composed of a hyperbolic contraction preceded by a post array. These predictions will then be compared to the experimental results of Balducci and Doyle,[20] establishing when the model performs well and when it does not. Finally, in cases where the numerical results are not accurate, reasons for the poor performance will be hypothesized.

II. BACKGROUND

A. Polymer deformation in field gradients

Electric fields are useful for stretching DNA in microfluidic devices because locally they are purely extensional with no rotational component.[33] This is important because fields with a rota-

tional component, such as shear flows, can lead to periodic behavior where the molecule stretches, collapses, and stretches again.[34,35] Practically, this reduces the effectiveness of the stretching device, and theoretically, it complicates the analysis of the molecular behavior.

Extensional fields cause stretching when the field gradients deform the molecule faster than it can rearrange itself.[5] The time scale for this molecular rearrangement is the longest relaxation time τ. When the relaxation time is balanced against the characteristic strain rate $\dot{\varepsilon}$ of the field, the result is the Deborah number, $\mathrm{De}=\dot{\varepsilon}\tau$, which is the governing dimensionless parameter for molecular deformation. It has been shown theoretically,[36] and confirmed experimentally,[15,37] that strong stretching occurs around $\mathrm{De}=0.5$.

A crude, but effective, model to describe DNA stretching in a homogeneous extensional field can be built using a simple dumbbell. By balancing the drag forces against the wormlike chain spring force[38] and neglecting Brownian motion and any other forces, the dynamic equation for the stretch can be expressed as

$$\frac{d}{d\varepsilon}\left(\frac{X}{L}\right)=\frac{X}{L}-\frac{1}{3\,\mathrm{De}}\left[\frac{1}{4(1-X/L)^2}-\frac{1}{4}+\frac{X}{L}\right], \tag{1}$$

where X is the extension of the molecule, L is the contour length, and ε is the applied strain. This model is particularly useful for predicting the final stretch of a DNA molecule after it has reached steady state, i.e., after an infinite amount of strain has been applied.

One of the greatest difficulties in stretching molecules in an extensional field is overcoming molecular individualism.[21] This phenomenon was first observed in early fluorescent microscopy work on DNA (Refs. 15 and 37) and refers to the fact that the initial conformation of a molecule greatly affects its rate of stretching. This often leads to a broad distribution of molecular extensions in stretching devices because each molecule has reached a different stage of deformation. Large amounts of strain ($\approx$10 units) (Ref. 39) are typically needed to uniformly stretch a population of molecules initially in their equilibrium state. This amount of strain is difficult to apply in most devices unless a field with a stagnation point is employed;[15,37,40,41] however, stagnation points typically cannot be used for high-throughput devices.

B. Model assumptions

We briefly consider the theory of DNA electrophoresis which underlies the assumptions of the numerical model. First, the electric field in the device can be determined by solving Laplace's equation because the buffer solution is assumed to be everywhere electroneutral. This assumption is valid because the Debye length κ^{-1} of the solution is typically $O(\mathrm{nm})$ which is much smaller than any other length scale in the problem. Additionally, we neglect any local disturbances of the electric field due to the charged phosphate backbone of DNA because, again, κ^{-1} is smaller than the molecule's persistence length, $A_p=0.053$ μm,[42] the smallest pertinent length scale of the polymer. This allows us to assume that DNA behaves as a neutral polymer without intramolecular electrostatic interactions.[43] We also assume the applied electric fields are weak and that we can neglect any nonlinear electrokinetic phenomena (although we will later question this assumption).

We invoke the theory of electro-hydrodynamic equivalence[44,45] which states that in the case of small Debye lengths, DNA dynamics in an electric field $\boldsymbol{E}$ can be treated the same as if the electric field were replaced with a hydrodynamic flow field equal to $\mu\boldsymbol{E}$, where μ is the electrophoretic mobility. This is due to the fact that flow disturbances in the fluid caused by the electrophoretic movement of DNA segments are screened over κ^{-1} due to the opposite movement of the surrounding counterion cloud.[1] Finally, we neglect all other forms of hydrodynamic interactions (HI) as the bulk radius of gyration of T4-DNA which was studied here ($R_g=1.4$ μm) is comparable to the channel height $h=2$ μm.[46]

C. Device geometry

The device we simulated is identical to that used by Balducci and Doyle[20] and is shown in Fig. 1(b). It consists of two straight channels of different widths connected by a hyperbolic

contraction. The wide inlet channel has a width of $w_1=200$ μm, and the outlet channel has a width of $w_2=3.8$ μm. The shape of the hyperbolic contraction was chosen to create a uniform strain rate within the contraction[17,19] and has a length of $\ell_c=80$ μm. In front of the contraction are three rows of posts with each post having a 1 μm radius. The posts are spaced 4 μm center-to-center within each row, and the distance between rows is also 4 μm center-to-center. The center of the first (most upstream) row of posts is located 20 μm in front of the contraction at $x=-20$ μm with the subsequent rows located at $x=-16$ μm and $x=-12$ μm. Finally, the corners of the device were rounded with a 1 μm radius.

The electrophoretic strain rate $\dot{\varepsilon}$ is nearly constant in much of the contraction,[18,19] and the nominal strain accumulated by a molecule moving down the centerline of the device is $\varepsilon \approx \ln(w_1/w_2)=4$. The electric field gradient in the contraction can be approximated using the scaling $\nabla E \approx (E_2-E_1)/\ell_c=[E_1(w_1/w_2-1)]/\ell_c$ where E_1 and E_2 are the electric field strengths at the inlet and the outlet of the channel, respectively. This leads to the form of the Deborah number within the contraction:

$$\mathrm{De}=\frac{\mu E_1(w_1/w_2-1)}{\ell_c}\tau. \tag{2}$$

Additional Deborah numbers can also be defined just before the post array and within the array,[20] but we do not consider them here. Finally, the kinematic history is not the same for each streamline.[19] Molecules that enter the contraction from the center of the channel deform differently than those that enter from the edges of the channel. In order to mitigate this effect, we adopted the method used by Balducci and Doyle[20] and only considered molecules whose centers of mass were within 45 μm of the center line when they entered the post array.

III. SIMULATIONS

We used a simulation method for DNA electrophoresis in arbitrary geometries that was developed by Kim and Doyle.[32] The method uses Brownian dynamics (BD) to model the behavior of a DNA molecule electrophoresing in an electric field. In order to solve for the electric field in complicated geometries, the finite element method (FEM) is employed. A difficulty that Kim and Doyle[32] addressed is how to find the electric field at an arbitrary point in the solution domain given that the finite element mesh is unstructured. They developed an efficient way to overcome this problem with the so-called "target-induced searching algorithm." A brief description of the numerical model is presented here.

A. Brownian dynamics

DNA molecules are modeled as chains of N_b beads connected by $N_s=(N_b-1)$ springs. The equation of motion for the position $\boldsymbol{r}_i$ of the ith bead is

$$\frac{d\boldsymbol{r}_i}{dt}=\mu^b\boldsymbol{E}(\boldsymbol{r}_i)+\frac{1}{\zeta^b}[\boldsymbol{F}_i^B(t)+\boldsymbol{F}_i^S(t)+\boldsymbol{F}_i^{EV}(t)+\boldsymbol{F}_i^{EV,wall}(t)], \tag{3}$$

where μ^b is the electrophoretic mobility of a bead, ζ^b is the bead drag coefficient, $\boldsymbol{F}_i^B$ is the Brownian force, $\boldsymbol{F}_i^S$ is the total spring force felt by the bead, $\boldsymbol{F}_i^{EV}$ is the intrachain excluded volume force due to nearby beads, and $\boldsymbol{F}_i^{EV,wall}$ represents the interaction of the bead with the wall of the device.

We nondimensionalize the variables as follows:

$$\hat{\boldsymbol{r}}\equiv\frac{\boldsymbol{r}}{l_s},\quad \hat{t}\equiv\frac{t}{\zeta^b l_s^2/k_BT},\quad \hat{\boldsymbol{E}}\equiv\frac{\boldsymbol{E}}{E_1}, \tag{4}$$

where $\boldsymbol{r}$ is position, l_s is the maximum extension of a single spring ($l_s\equiv L/N_s$), t is time, k_B is Boltzmann's constant, and T is the absolute temperature. We nondimensionalize the forces $\boldsymbol{F}$ as follows:

$$\hat{\boldsymbol{F}}(\hat{\boldsymbol{r}}) \equiv \frac{\boldsymbol{F}}{k_{\mathrm{B}}T/l_{\mathrm{s}}}. \tag{5}$$

This leads to the nondimensional form of Eq. (3),

$$\frac{d\hat{\boldsymbol{r}}_i}{d\hat{t}} = \mathrm{Pe}^{\mathrm{b}}\hat{\boldsymbol{E}}(\hat{\boldsymbol{r}}_i) + \hat{\boldsymbol{F}}_i^{\mathrm{B}} + \hat{\boldsymbol{F}}_i^{\mathrm{S}} + \hat{\boldsymbol{F}}_i^{\mathrm{EV}} + \hat{\boldsymbol{F}}_i^{\mathrm{EV,wall}}, \tag{6}$$

where Pe^{b} is the bead Peclet number ($\mathrm{Pe}^{\mathrm{b}} \equiv \mu^{\mathrm{b}}E_1 l_{\mathrm{s}}/D^{\mathrm{b}}$) given that the bead diffusivity $D^{\mathrm{b}} = k_{\mathrm{B}}T/\zeta^{\mathrm{b}}$. The nondimensional Brownian force is given by

$$\hat{\boldsymbol{F}}_i^{\mathrm{B}} = \sqrt{\frac{24}{\Delta\hat{t}}}(\boldsymbol{r}_n)_i, \tag{7}$$

where $\Delta\hat{t}$ is the dimensionless time step and $(\boldsymbol{r}_n)_i$ are uniform random numbers such that each component $(\boldsymbol{r}_n)_i^j \in [-1/2, 1/2]$, where j denotes the coordinate x, y, or z. The net nondimensional spring force on the ith bead is

$$\hat{\boldsymbol{F}}_i^{\mathrm{S}} = \begin{cases} \hat{\boldsymbol{f}}_{i,2}^{\mathrm{s}}, & i = 1, \\ \hat{\boldsymbol{f}}_{i,i+1}^{\mathrm{s}} + \hat{\boldsymbol{f}}_{i,i-1}^{\mathrm{s}}, & 1 < i < N_{\mathrm{b}}, \\ \hat{\boldsymbol{f}}_{i,N_{\mathrm{b}}-1}^{\mathrm{s}}, & i = N_{\mathrm{b}}, \end{cases} \tag{8}$$

where the spring force $\hat{\boldsymbol{f}}_{i,j}^{\mathrm{s}}$ is given by a modified Marko-Siggia spring force law:[38,47]

$$\hat{\boldsymbol{f}}_{i,j}^{\mathrm{s}} = \frac{\upsilon}{\lambda}\left[\hat{r}_{ji} - \frac{1}{4} + \frac{1}{4(1-\hat{r}_{ji})^2}\right]\frac{\hat{\boldsymbol{r}}_j - \hat{\boldsymbol{r}}_i}{\hat{r}_{ji}}, \tag{9}$$

where λ is the ratio of the effective persistence length to the true persistence length ($\lambda \equiv A_{\mathrm{eff}}/A_{\mathrm{p}}$), υ is the number of true persistence lengths represented by each spring ($\upsilon \equiv l_{\mathrm{s}}/A_{\mathrm{p}}$), and $\hat{r}_{ji}$ represents the distance between $\hat{\boldsymbol{r}}_j$ and $\hat{\boldsymbol{r}}_i$. The intrachain excluded volume force $\hat{\boldsymbol{F}}_i^{\mathrm{EV}}$ is modeled with the soft potential used by Jendrejack *et al.*:[48]

$$\hat{\boldsymbol{F}}_i^{\mathrm{EV}} = -\sum_{j=1(j\neq i)}^{N_{\mathrm{b}}} \frac{9}{2}\hat{\nu}^{\mathrm{ev,p}}\left(\frac{3}{4\sqrt{\pi}}\right)^3 \upsilon^{9/2} \exp\left[-\frac{9}{4}\upsilon\hat{r}_{ij}^2\right]\hat{\boldsymbol{r}}_{ji}, \tag{10}$$

where $\hat{\nu}^{\mathrm{ev,p}} \equiv \nu^{\mathrm{ev,p}}/l_{\mathrm{s}}^3$ is the dimensionless form of the excluded volume parameter $\nu^{\mathrm{ev,p}}$.

The interactions between a bead and the walls represented by $\hat{\boldsymbol{F}}_i^{\mathrm{EV,wall}}$ are resolved using a modified Heyes-Melrose algorithm.[32,49] Whenever a bead moves outside the domain during a time step, it is moved to the nearest point on the domain boundary before commencing the next time step:

$$\Delta\hat{\boldsymbol{r}}_i^{\mathrm{HM}} = \Delta\boldsymbol{p}_i H(\Delta p_i), \tag{11}$$

where $\Delta\hat{\boldsymbol{r}}_i^{\mathrm{HM}}$ is the displacement vector due to the Heyes-Melrose algorithm, $\Delta\boldsymbol{p}_i$ is the vector pointing from the bead outside the domain to the nearest boundary point, and the Heaviside step function $H(\Delta p_i)$ restricts the application of the algorithm to only the beads that have penetrated the domain boundaries.

B. Determination of electric field

In order to determine the electric field in the device, we use Laplace's equation for the electric potential ϕ within the channel as previously discussed,

$$\nabla^2 \phi = 0. \tag{12}$$

We assume that the polydimethylsiloxane (PDMS) channel walls are insulating and that the electric fields at the device inlet and outlet are uniform. This leads to the boundary conditions

$$\phi|_{\text{inlet}} = \phi_1, \quad \phi|_{\text{outlet}} = \phi_2, \text{ and } \boldsymbol{n} \cdot \nabla \phi|_{\text{walls}} = 0, \tag{13}$$

where ϕ_1 and ϕ_2 are the imposed electric potentials at the inlet and the outlet of the device, respectively, and $\boldsymbol{n}$ is the unit normal to the walls.

Equations (12) and (13) are solved using Galerkin FEM where ϕ is interpolated using a six-node P_2^0 shape function. The electric field $\boldsymbol{E}$ is found by applying FEM again to the relation $\boldsymbol{E} = -\nabla \phi$ and using a three-node P_1^0 shape function to interpolate $\boldsymbol{E}$. After obtaining $\boldsymbol{E}$, its nodal values are saved. During the simulations, whenever the value of $\boldsymbol{E}$ is needed at a given point, the target-induced searching algorithm is called to find the element in which the point is located. The nodal values for $\boldsymbol{E}$ in that element are then retrieved, and the value of $\boldsymbol{E}$ at the specified point is interpolated.

C. Parameters

In this study, T4-DNA was modeled in the same manner as Kim and Doyle[32] in their simulations of DNA collisions with a single post. They assumed a stained contour length of $L = 71.4$ μm and used $N_b = 128$ beads such that $\upsilon = 10.61$. The corresponding λ was 1.89, and an excluded volume parameter $\nu^{\text{ev,p}}$ of 0.0004 μm^3 was found to accurately reproduce the radius of gyration of λ-DNA. At this discretization, along with sufficiently small time steps, the aphysical situation where a chain can move "through" a post is precluded. We found the simulated nondimensional relaxation time of the 128-bead chain to be $\hat{\tau} = 60.1$ in a 2 μm tall channel.

Due to the low field strengths in the inlet of the channel, it takes a very long time to simulate the movement of a chain from the inlet to the beginning of the contraction. In order to decrease the simulation time, point particles possessing the same diffusivity as the 128-bead chains were placed at $x/\ell_c = -2$ and were distributed randomly across the width of the channel with a uniform distribution. The movement of the particles toward the contraction was then simulated until the local dimensionless strain rate $\hat{\dot{\varepsilon}} = l_s^2 \dot{\varepsilon} / D_b$ along the centerline reached $\hat{\dot{\varepsilon}} = 0.1/\hat{\tau}$ (but no farther than $x = -30$ μm for the low De cases). At this point, equilibrated chains were placed with their center of masses located at the positions of the particles. The electrophoresis of the chains was then simulated until the most downstream part of the chains reached $x = 250$ μm. The time step scheme was as follows: $\Delta \hat{t} = 0.005$ for $x < -24$ μm at which point it switched to

$$\Delta \hat{t} = \begin{cases} 0.005, & \text{De} < 3, \\ 0.005\left(\dfrac{3}{\text{De}}\right), & \text{De} \geqslant 3. \end{cases} \tag{14}$$

For each De considered, 300 chains were simulated although only those within 45 μm of the centerline when they entered the post array were used in this study as discussed earlier.

IV. RESULTS

The major global observable in the study was the average extension of the molecules as they reached the end of the contraction. In our simulations, the extension of a chain X_{ex} is defined as the distance between the most upstream and downstream beads of the chain, and the extension at the end of the contraction $X_{\text{ex,c}}$ was determined when the most downstream part of the chain first passed the end of the contraction. Figure 2 compares results from experiments and simulations for $X_{\text{ex,c}}$. It is clear from Fig. 2(a) that the simulation model does an excellent job of predicting the mean stretch of the molecules in an open channel as was previously shown by Kim and Doyle.[32]

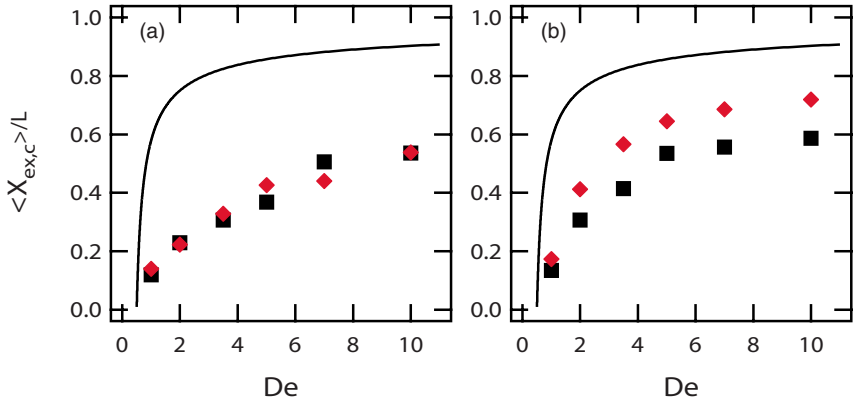

FIG. 2. Ensemble-averaged relative stretch of the chains as they reach the end of the contraction vs De (a) in an open channel and (b) in a channel with posts. The black squares are the experimental data, and the red diamonds are the simulation data. The line represents the theoretical infinite-strain stretch as predicted by the simple dumbbell model given in Eq. (1). The error bars, which have been suppressed for clarity, are approximately the size of the markers themselves.

But when posts are introduced in front of the contraction, the simulations consistently over predict the average extension by 10–15 % as shown in Fig. 2(b). Nonetheless, the results are in qualitative agreement with the experimental trend.

In order to explore why the performance of the simulation model changes so abruptly when posts are added, we have attempted to isolate and analyze the behavior of the chains in each component of the device, i.e., the post array and the contraction. Although this is not strictly possible because the effects of each are certainly coupled, it still provides clues as to why the simulations and experiments differ. In particular, we are interested in whether the differences between the two are simply due to quantitative inaccuracies within the numerical model or due to the failure of the model to predict qualitative features of the experiments.

A. Interactions with the post array

To assess the ability of the simulations to correctly describe the interactions between the molecules and the posts, we calculated chain hooking probabilities. A hook was defined as when portions of the chain exist in all four quadrants surrounding a post in a coordinate system whose origin is located at the center of the post; in addition, the chain must cross the upstream face of the post. Unlike in experiments, the coordinate system used to define the quadrants was not rotated to coincide with the direction of the local impinging electric field; however, this was not found to affect the determination of a hooking event. Figure 3 shows the results of this hooking analysis. The overall hooking probabilities on any post (a) show near quantitative agreement between the experiments and simulations except at De=1 and 2 where the simulations give a moderate over prediction. The probability of hooking on the first row is also shown (b), and again there is near quantitative agreement except at De=2.

It should be noted that the hooking probability on a post is known to depend on both the local De and Pe.[24,33] In the simulations, however, only a single time scale can be matched to experiments which, in this case, is the relaxation time. This means that while De is the same between experiments and simulations, other time scales are not necessarily equivalent. This includes the diffusive time scale which is represented nondimensionally by Pe. Indeed, we estimate Pe for the simulations is 15–40 % higher than in experiments. This difference in Pe might account for some of the discrepancy between the hooking probabilities in experiments and simulations at De=1 and 2. A better explanation, however, is that the number of experimental hooking events were undercounted at low De due to the limited resolution of images and the fact that many molecules barely deformed around the posts in the weak fields. This explanation is supported by movies of the simulated chains where many hooking events are seen to barely meet the above definition of a

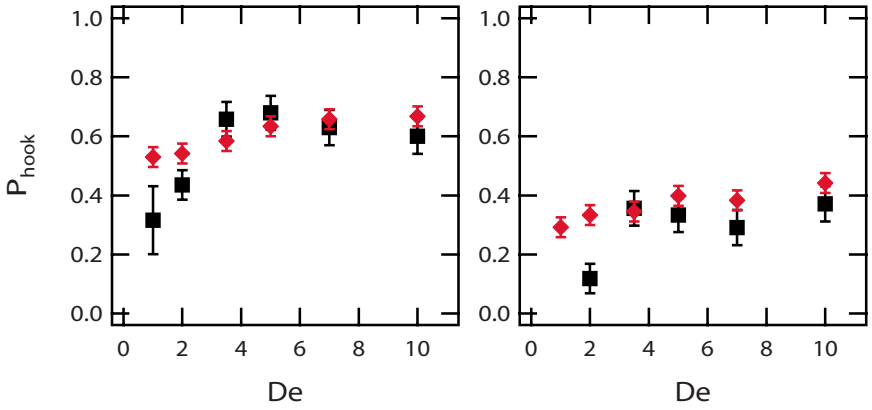

FIG. 3. (a) Overall hooking probabilities on all rows in the post array vs De. (b) The hooking probabilities for only the first row of the array vs De. The black squares are the experimental data, and the red diamonds are the simulation data.

hook with the chains just crossing into all four quadrants surrounding the post for a very short period of time. Simulations easily find and count this event as a hook while the reliability of experimental movie analysis is questionable at low field strengths.

An even more sensitive measure of the performance of the simulation model in predicting the DNA-post array interactions is given by the extension distribution of the chains as they leave the array. The extension $X_{ex,p}$ of the chains was measured when the most upstream part of the chain first left the post array. Figure 4 compares the extension distributions for experiments and simulations, and very good qualitative agreement is evident with the exception of De=5. It is seen that with increasing electric field strength, the presence of the obstacle array leads to two distinct populations of molecules: those that only mildly stretch in the array and those that stretch signifi-

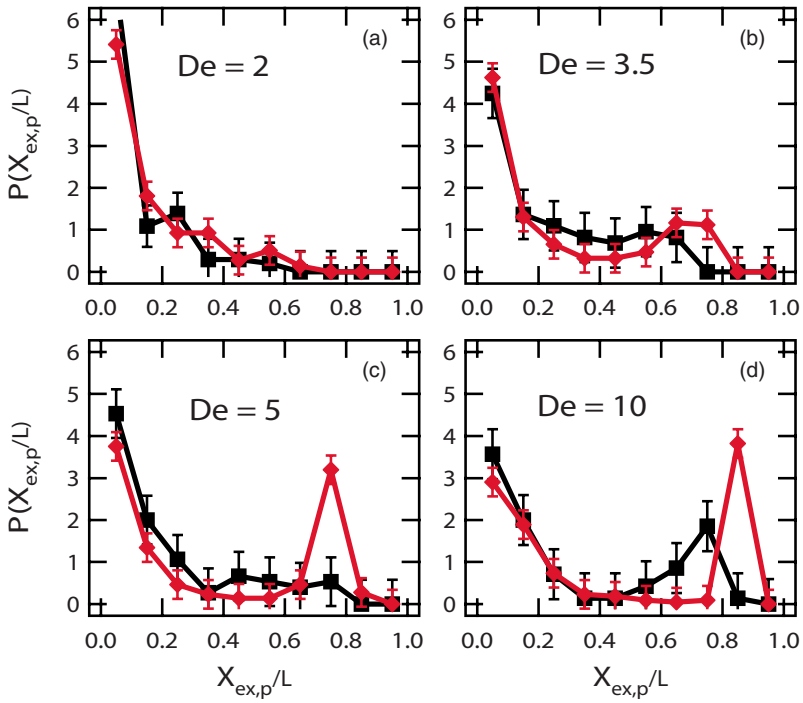

FIG. 4. Distribution of the relative extensions of the chains as they pass the end of the post array for several values of De. The black squares are the experimental data and the red diamonds are the simulation data.

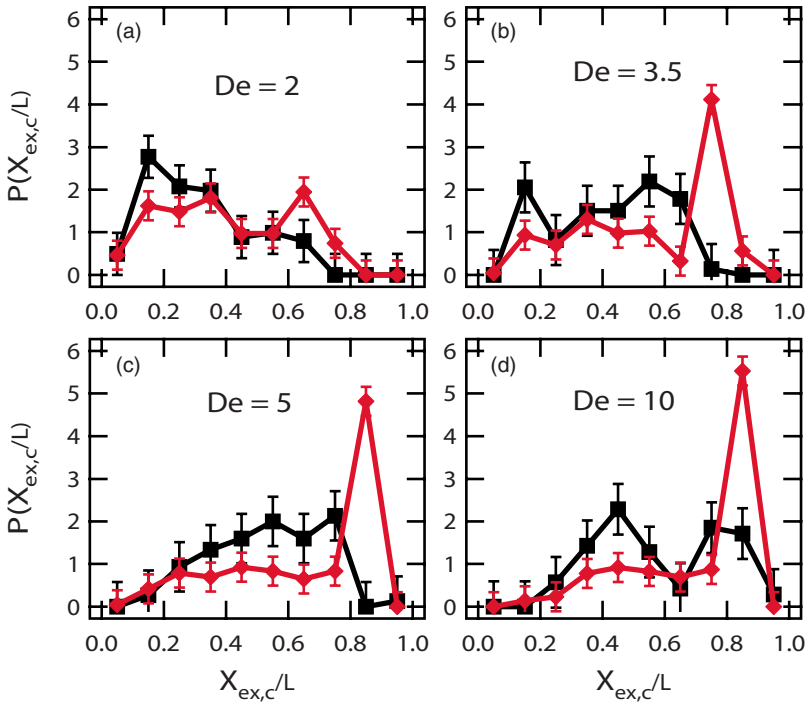

FIG. 5. Distribution of the relative extensions of the chains as they reach the end of the contraction for several values of De. The black squares are the experimental data and the red diamonds are the simulation data.

cantly. Very few molecules stretch only moderately. Quantitatively, the simulations tend to show a sharper peak for the highly stretched population which also exists at a slightly higher extension, but this difference could be magnified by the simulations having a slightly higher Pe as previously discussed. But due to poor statistics, it is difficult to discern the actual behavior of the distributions at the experimental conditions of De=3.5 and 5. Another consideration is that as the molecules unhook, their arms often hang off into the contraction. This means that the stretch leaving the post array is influenced by the behavior in the contraction. If the simulations have difficulty correctly predicting the stretch due to the field gradients in the contraction, it can taint the stretch coming off the post array as well.

Overall, we see that qualitatively, and often quantitatively, the experiments and simulations agree with respect to the behavior of the molecules as they interact with the post array. This is expected as Kim and Doyle[28] have shown the simulation model is fairly capable of reproducing experimental data for the collision of a molecule with a single post. Additionally, other Brownian dynamics simulation methods have had success reproducing the behavior of DNA being hydrodynamically driven through post arrays.[14]

B. Stretching in the contraction

We now consider the extension distributions of the chains as they reach the end of the contraction as shown in Fig. 5. The simulations show that with increasing De more chains reach high extensions, in agreement with experimental results. However, simulations show a very sharp peak in the distribution at high extensions which is not mirrored in the experimental results. This discrepancy cannot be explained by unmatched Pe, and while poor experimental statistics may exacerbate the differences, statistics certainly cannot fully account for the discrepancies either, especially given their systematic nature. This suggests that the molecules are somehow more difficult to stretch in experiments than in simulations. However, it is also possible that the slightly higher extensions coming off the post array in the simulations could increase the final stretch at the end of the contraction.

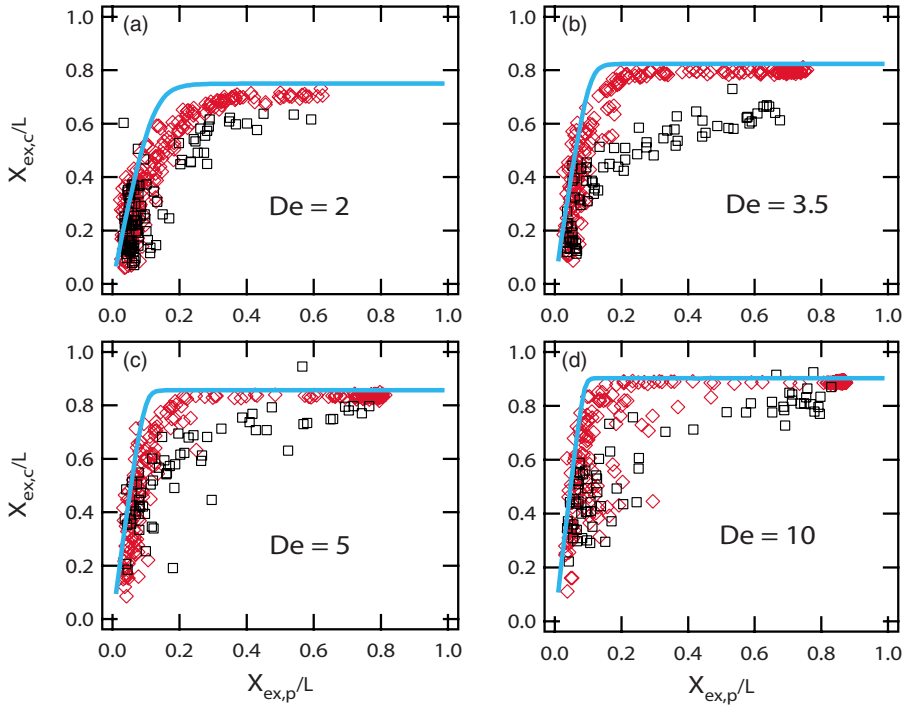

FIG. 6. Scatter plots of the relative extension of the chains when they reach the end of the contraction vs the relative extension when the chains exit the post array for various De. The black squares are the experimental data and the red diamonds are the simulation data. The solid blue line represents the predicted final stretch after an additional 2.5 units of strain using the dumbbell model given by Eq. (1).

In order to mitigate the influence of the post array on the analysis of the stretching within the contraction, we display in Fig. 6 scatter plots that show for each chain the final stretch at the end of the contraction versus the intermediate stretch at the exit of the post array. This allows us to compare the deformation of molecules in the contraction that had the same initial stretch leaving the array. Again, the simulations are in qualitative agreement with experiments that DNA deformation in the post array leads to very strong stretching in the contraction. In particular, the simulations predict that a stretch of approximately 20% at the exit of the post array virtually guarantees strong stretching at the end of the contraction and additional predeformation beyond 20% adds little to the final stretch, as previously discovered in experiments.

On the other hand, there are some clear differences between the two results. First, the simulated chains seem to reach a larger maximum extension than molecules in experiments. This may suggest that De is not properly matched, but it is highly unlikely. The maximum extension found in the simulations is well described by the infinite-strain limit predicted by a dumbbell model with the same De (the flat plateau region of the blue curve in Fig. 6), and experimentally, even if De is off slightly due to uncertainty in the relaxation time of the molecules, correcting this small error would not change De enough to match the simulations. So simply claiming that the differences in maximum stretch are due to improperly matched time scales does not explain the differences.

The second discrepancy observed in Fig. 6 is that the simulations predict that above a predeformation of about 20% the chains should almost always reach their maximum extension. This gives the stretch gain plots from simulations of De $\geqslant$ 3.5 [Figs. 6(b)–6(d)] a sharp "elbow" region where the trend turns flat. In contrast, experimental results show that the molecules often fall slightly short of their infinite-strain extension. Also, the amount the actual extension falls below the infinite-strain extension decreases with increasing predeformation. This leads to a wider elbow region in the stretch gain plots where the trend becomes slowly increasing instead of constant as in simulations. In order to demonstrate that our simulation results make sense based on the physics

incorporated, we have included in Fig. 6 a prediction for the maximum stretch gain expected at the end of the contraction for a given amount of predeformation. This prediction was derived using the non-Brownian dumbbell model with a wormlike chain (WLC) spring force given by Eq. (1). Based on the kinematic analysis of Randall *et al.*,[18] we have assumed that after the post array there is approximately 2.5 units of strain left in the device. The model accounts for nonaffine deformation of the chains, but does not include resistance to stretching due to internal configurations (i.e., molecular individualism) or the slightly different kinematic histories experienced by each chain. Nonetheless, it should provide a reasonable estimate for the maximum stretch gain expected. It is clearly seen from Fig. 6 that the simulation results are well described by the model while the experimental results only follow its qualitative trends.

Balducci and Doyle[20] also reported that many of the molecules in the elbow region, $0.2 < X_{ex,p}/L < 0.4$, contained a small fold in their conformation near their downstream ends as they exited the contraction. The simulations do not predict this behavior since nearly all the molecules in this extension range after the post array will reach the infinite-strain limit. Indeed, movies of the simulated chains do not show the formation of these folded conformations.

Overall, our numerical model is capable of reproducing the broad qualitative behavior of the chains in the contraction after they have left the post array. For example, the simulations predict that mildly predeformed chains should stretch significantly in the contraction in agreement with experiments. However, the simulations do not correctly predict some of the finer qualitative behavior in the contraction.

C. Possible reasons for the observed differences

The question, then, is why the simulation results do not always quantitatively match the results of the experiments? One possible reason already mentioned could be limited experimental statistics. But the systematic nature of the differences between simulations and experiments suggest that these differences are not artificial. A mismatch in time scales has also been discussed as one reason. This mismatch could be an improperly scaled De due to uncertainties in the relaxation time of the molecules, or it could be the slightly higher Pe in the simulations due to the inability of the simulations to match both the relaxation time and the diffusive time scale of experiments. However, neither of these possibilities has the potential to fully explain the differences seen.

A more plausible explanation is that additional physics is becoming important in the contraction, and a possible candidate is nonlinear electrokinetic effects. The electric fields in the contraction are fairly strong, reaching $E \sim O(500\ \mathrm{V/cm})$, which could polarize the DNA molecules. Additionally, electric field gradients exist in the contraction that could potentially lead to dielectrophoretic effects which depend upon the term $\boldsymbol{E}\cdot\nabla\mathbf{E}$.

Dielectrophoresis occurs when particles (or macromolecules) polarize in strong electric fields. The resulting dipole then interacts with field gradients to attract or repel the particles to or from areas of strong field strengths. Most studies on the dielectrophoresis of DNA have used ac fields and created the necessary electric field gradients by placing the electrodes in close proximity to each other. There have been a few studies, however, that have considered electrodeless dielectrophoresis of DNA using microfabricated devices to shape the field lines,[50–53] and some work has even been performed on dc fields.[52,53]

Chou *et al.*[50] and Regtmeier *et al.*[51] used arrays of obstacles to bend and concentrate the field lines between the obstacles, and using an ac field, they trapped DNA between the obstacles. Regtmeier *et al.* also added a background dc field that led to the size-dependent separation of DNA molecules. This technique is similar to the previously proposed method of Ajdari and Prost[54] where ac dielectrophoretic traps transverse to a uniform dc field slow down DNA molecules in a size-dependent manner. Petersen *et al.*[52] also adapted the method suggested by Ajdari and Prost by using thin strips of gold laid down perpendicular to a dc electric field. The periodic strips attracted the electric field lines due to their high conductivity and created strong dielectrophoretic forces in a highly localized area near the edges of the gold strips. Parikesit *et al.*[53] used device walls to bend and concentrate field lines similar to Chou *et al.*[50] but with dc fields; however, their results were difficult to interpret and even seemed to contradict previous findings.

In our device, the magnitude of $\boldsymbol{E}\cdot\nabla\mathbf{E}$ reaches as high as 1.4×10^{7} $\mathrm{V}^2/\mathrm{cm}^3$ which is only one order of magnitude smaller than that produced by Petersen *et al.*[52] in their trapping work. But in contrast to our device, the large values of $\boldsymbol{E}\cdot\nabla\mathbf{E}$ that led to trapping were highly localized near the edges of the gold strips and only occurred over length scales of about 100 nm, comparable to the persistence length of DNA. This means that only small portions of the molecules would have been polarized and would have experienced a dielectrophoretic force. In our geometry, the strong fields and gradients exist over the entire length of the contraction which is $\ell_c=80$ μm, which is much larger than the radius of gyration of T4-DNA and comparable to its contour length. So T4-DNA molecules in our device could polarize over their entire dimension which could possibly lead to even stronger nonlinear electrokinetic effects than seen by Petersen *et al.*[52] In addition, the fact that DNA molecules are stretched in the contraction could render them more polarizable than when they are in their coiled state,[55] further increasing their sensitivity to nonlinear electrokinetic effects.

It is currently difficult to study the possibility of such effects in the device because the molecules move very fast through the contraction due to the strong electric fields. A possible way to overcome this problem would be to tether the DNA molecule to a bead that can be optically trapped in the contraction so that the dynamic and steady-state extension behavior of the molecule can be studied.

Finally, it should again be noted that the current simulation model is able to match experimental results for a contraction without posts which raises the question, what is different about the situation with posts? The answer may lie in the fact that in an open channel, few of the chains actually come close to reaching the infinite-strain limit extension. Even in the case with posts, the simulations seem to be in fairly good agreements with experiments for those chains that do not stretch significantly. Additionally, in the case of open channels, the simulations have been shown to over predict the average stretch at higher De of 14 and 23 when compared to experiments.[19] At these De, the simulations began to over predict the populations of highly stretched molecules; however, the size of this population still only represented a small fraction of the total number of molecules. So any discrepancy in the behavior of highly stretched molecules between the simulations and experiments may not have been readily apparent. In the present situation, preconditioning leads to a large population of highly stretched molecules so that these differences should be more easily visible.

V. CONCLUSIONS

Simulations were performed for DNA molecules passing through a microcontraction preceded by a post array. The results were compared to those from previously performed experiments. Good qualitative and, at times, even quantitative agreement was found for the behavior of the chains during their interaction with the post array as measured by hooking probabilities and extension distributions of the chains as they exited the array. Qualitatively, the simulations strongly support the experimental finding that conformational preconditioning using an obstacle array can increase the stretching efficiency of a strain-limited microcontraction. Additionally, the simulations show that a predeformation of approximately 20% in the post array is nearly sufficient to guarantee strong stretching of a chain in the contraction in accordance with experiments.

Qualitative differences between the simulations and experiments were observed, particularly with respect to the population of highly stretched molecules. The simulations predict a very sharp peak in the extension distribution at high extensions for the molecules exiting the contraction while experimental results exhibited a broader and milder peak at high extensions. This difference causes simulations to over predict the average stretch of the molecules leaving the contraction. Finally, the molecules in experiments always seemed to fall slightly short of the infinite-strain limit extension while simulations predict that nearly all molecules that left the post array with an extension above 20% would reach the infinite-strain limit by the end of the contraction. Possible reasons for the discrepancy between simulations and experiments are suggested with emphasis on nonlinear electrokinetic effects. Additionally, experiments which might elucidate the behavior of molecules in the contraction are suggested.

ACKNOWLEDGMENTS

The authors are grateful to Anthony Balducci and Jing Tang for many helpful discussions. This work was supported by the Singapore-MIT Alliance and by Award No. T32EB006348 from the National Institute of Biomedical Imaging and Bioengineering. The content is solely the responsibility of the authors and does not necessarily represent the official views of the National Institute of Biomedical Imaging and Bioengineering or the National Institutes of Health.

[1] J. L. Viovy, Rev. Mod. Phys. **72**, 813 (2000).
[2] E. Y. Chan, N. M. Goncalves, R. A. Haeusler, A. J. Hatch, J. W. Larson, A. M. Maletta, G. R. Yantz, E. D. Carstea, M. Fuchs, G. G. Wong, S. Gullans, and R. Gilmanshin, Genome Res. **14**, 1137 (2004).
[3] K. M. Phillips, J. W. Larson, G. R. Yantz, C. M. D'Antoni, M. V. Gallo, K. A. Gillis, N. M. Goncalves, L. A. Neely, S. R. Gullans, and R. Gilmanshin, Nucleic Acids Res. **33**, 5829 (2005).
[4] J. O. Tegenfeldt, O. Bakajin, C. F. Chou, S. S. Chan, R. Austin, W. Fann, L. Liou, E. Chan, T. Duke, and E. C. Cox, Phys. Rev. Lett. **86**, 1378 (2001).
[5] P.-G. de Gennes, *Scaling Concepts in Polymer Physics* (Cornell University Press, Ithaca, NY, 1979).
[6] J. O. Tegenfeldt, C. Prinz, H. Cao, S. Chou, W. W. Reisner, R. Riehn, Y. M. Wang, E. C. Cox, J. C. Sturm, P. Silberzan, and R. H. Austin, Proc. Natl. Acad. Sci. U.S.A. **101**, 10979 (2004).
[7] R. Riehn, M. C. Lu, Y. M. Wang, S. F. Lim, E. C. Cox, and R. H. Austin, Proc. Natl. Acad. Sci. U.S.A. **102**, 10012 (2005).
[8] S. B. Smith, L. Finzi, and C. Bustamante, Science **258**, 1122 (1992).
[9] T. R. Strick, J. F. Allemand, D. Bensimon, A. Bensimon, and V. Croquette, Science **271**, 1835 (1996).
[10] T. T. Perkins, D. E. Smith, R. G. Larson, and S. Chu, Science **268**, 83 (1995).
[11] M. D. Wang, H. Yin, R. Landick, J. Gelles, and S. M. Block, Biophys. J. **72**, 1335 (1997).
[12] W. D. Volkmuth and R. H. Austin, Nature (London) **358**, 600 (1992).
[13] N. Minc, C. Futterer, K. Dorfman, A. Bancaud, C. Gosse, C. Goubault, and J. L. Viovy, Anal. Chem. **76**, 3770 (2004).
[14] N. P. Teclemariam, V. A. Beck, E. S. G. Shaqfeh, and S. J. Muller, Macromolecules **40**, 3848 (2007).
[15] T. T. Perkins, D. E. Smith, and S. Chu, Science **276**, 2016 (1997).
[16] E. S. G. Shaqfeh, J. Non-Newtonian Fluid Mech. **130**, 1 (2005).
[17] J. W. Larson, G. R. Yantz, Q. Zhong, R. Charnas, C. M. D'Antoni, M. V. Gallo, K. A. Gillis, L. A. Neely, K. M. Phillips, G. G. Wong S. R. Gullans, and R. Gilmanshin, Lab Chip **6**, 1187 (2006).
[18] G. C. Randall, K. M. Schultz, and P. S. Doyle, Lab Chip **6**, 516 (2006).
[19] J. M. Kim and P. S. Doyle, Lab Chip **7**, 213 (2007).
[20] A. Balducci and P. S. Doyle, Macromolecules **41**, 5485 (2008).
[21] P. G. de Gennes, Science **276**, 1999 (1997).
[22] R. G. Larson, J. Non-Newtonian Fluid Mech. **94**, 37 (2000).
[23] W. D. Volkmuth, T. Duke, M. C. Wu, R. H. Austin, and A. Szabo, Phys. Rev. Lett. **72**, 2117 (1994).
[24] G. C. Randall and P. S. Doyle, Macromolecules **38**, 2410 (2005).
[25] G. C. Randall and P. S. Doyle, Macromolecules **39**, 7734 (2006).
[26] G. I. Nixon and G. W. Slater, Phys. Rev. E **50**, 5033 (1994).
[27] P. M. Saville and E. M. Sevick, Macromolecules **32**, 892 (1999).
[28] J. M. Kim and P. S. Doyle, Macromolecules **40**, 9151 (2007).
[29] P. D. Patel and E. S. G. Shaqfeh, J. Chem. Phys. **118**, 2941 (2003).
[30] K. D. Dorfman, Phys. Rev. E **73**, 061922 (2006).
[31] A. Mohan and P. S. Doyle, Phys. Rev. E **76**, 040903 (2007).
[32] J. M. Kim and P. S. Doyle, J. Chem. Phys. **125**, 074906 (2006).
[33] G. C. Randall and P. S. Doyle, Phys. Rev. Lett. **93**, 058102 (2004).
[34] T. W. Liu, J. Chem. Phys. **90**, 5826 (1989).
[35] D. E. Smith, H. P. Babcock, and S. Chu, Science **283**, 1724 (1999).
[36] R. G. Larson and J. J. Magda, Macromolecules **22**, 3004 (1989).
[37] D. E. Smith and S. Chu, Science **281**, 1335 (1998).
[38] J. F. Marko and E. D. Siggia, Macromolecules **28**, 8759 (1995).
[39] R. G. Larson, H. Hu, D. E. Smith, and S. Chu, J. Rheol. **43**, 267 (1999).
[40] C. M. Schroeder, H. P. Babcock, E. S. G. Shaqfeh, and S. Chu, Science **301**, 1515 (2003).
[41] J. Tang and P. S. Doyle, Appl. Phys. Lett. **90**, 224103 (2007).
[42] C. Bustamante, J. F. Marko, E. D. Siggia, and S. Smith, Science **265**, 1599 (1994).
[43] J. L. Barrat and J. F. Joanny, Adv. Chem. Phys. **94**, 1 (1996).
[44] D. Long, A. V. Dobrynin, M. Rubinstein, and A. Ajdari, J. Chem. Phys. **108**, 1234 (1998).
[45] S. Ferree and H. W. Blanch, Biophys. J. **85**, 2539 (2003).
[46] A. Balducci, P. Mao, J. Han, and P. S. Doyle, Macromolecules **39**, 6273 (2006).
[47] P. T. Underhill and P. S. Doyle, J. Non-Newtonian Fluid Mech. **122**, 3 (2004).
[48] R. M. Jendrejack, J. J. de Pablo, and M. D. Graham, J. Chem. Phys. **116**, 7752 (2002).
[49] D. M. Heyes and J. R. Melrose, J. Non-Newtonian Fluid Mech. **46**, 1 (1993).
[50] C. F. Chou, J. O. Tegenfeldt, O. Bakajin, S. S. Chan, E. C. Cox, N. Darnton, T. Duke, and R. H. Austin, Biophys. J. **83**, 2170 (2002).
[51] J. Regtmeier, T. T. Duong, R. Eichhorn, D. Anselmetti, and A. Ros, Anal. Chem. **79**, 3925 (2007).
[52] E. Petersen, B. Q. Li, X. H. Fang, H. B. Luo, V. Samuilov, D. Gersappe, J. Sokolov, B. Chu, and M. Rafailovich, Phys. Rev. Lett. **98**, 088102 (2007).

[53] G. O. F. Parikesit, A. P. Markesteijn, O. M. Piciu, A. Bossche, J. Westerweel, I. T. Young, and Y. Garini, Biomicrofluidics **2**, 024103 (2008).
[54] A. Ajdari and J. Prost, Proc. Natl. Acad. Sci. U.S.A. **88**, 4468 (1991).
[55] J. S. Bowers and R. K. Prudhomme, J. Chem. Phys. **96**, 7135 (1992).